Dynamics of lossless polarization attraction

Matteo Barozzi* and Armando Vannucci

Dipartimento di Ingegneria Dell'Informazione, Università degli Studi di Parma, Viale delle Scienze 181/A, Parma 43124, Italy
**Corresponding author: matteo.barozzi82@gmail.com*

Received June 1, 2015; revised July 17, 2015; accepted July 21, 2015; posted July 23, 2015 (Doc. ID 242074); published August 21, 2015

We study a nonlinear lossless polarizer (NLP), a fiber-based device able to control the polarization of an optical signal while preserving its energy. The NLP exploits the lossless polarization attraction (LPA) generated by the Kerr interactions between the signal and a fully polarized continuous wave (CW) pump. By employing a copropagating pump, we show that the effectiveness of LPA depends on the joint action of the Kerr nonlinearity and the mutual delay between signal and pump. We find the optimal pump wavelength placement and demonstrate that true LPA occurs only within a limited range of delay values. Thus, we explain why the copropagating NLP is more flexible and power efficient compared with the traditional counterpropagating NLP. © 2015 Chinese Laser Press

OCIS codes: (060.4370) Nonlinear optics, fibers; (230.5440) Polarization-selective devices; (230.4320) Nonlinear optical devices; (230.1150) All-optical devices.
http://dx.doi.org/10.1364/PRJ.3.000229

1. INTRODUCTION

A nonlinear lossless polarizer (NLP) is a fiber-based device that performs all-optical control of the signal's state of polarization (SOP) by exploiting lossless polarization attraction (LPA) [1]. LPA is a Kerr-induced phenomenon such that any arbitrary signal SOP is attracted toward the SOP of a fully polarized continuous wave (CW) pump (with the well-known exception of a signal SOP orthogonal to the pump SOP). In the last decade, polarization-sensitive Kerr interactions have been used for a variety of applications, including ultrafast modulation techniques [2]. Since LPA preserves the signal intensity, NLP represents a promising solution for all-optical signal processing and telecom applications [3–5].

Indeed, the effectiveness of LPA strongly depends on the joint action between the Kerr interactions and the mutual delay, i.e., the *walk-off*, between signal and pump [6]. LPA with a counterpropagating pump requires long transient times (microseconds) and high signal peak power (watts) [7,8] due to the fixed and relativistic walk-off, and its simulation as a boundary value problem is time- and memory-intensive [9]. Instead, if signal and pump copropagate, their walk-off can be tuned and LPA transient times can be optimized for any given coherence time of the signal SOP [6]. Hence, a copropagating NLP can repolarize even signals with a fast-varying SOP, by employing lower peak power levels [10].

However, one of the objectives of this work is to show that despite the fact that the relevant parameters can differ by orders of magnitude, LPA occurs with the same dynamics in the two configurations. Here, we characterize numerically the performance of a copropagating NLP as a function of the signal–pump walk-off, and find the optimal pump wavelength that maximizes the effectiveness of LPA for given power levels. At the same time, we shall cast new light on the central role of walk-off in the LPA dynamics, by showing that appropriate tuning of the walk-off is necessary to reach the *polarization attraction regime*.

2. LPA

Figure 1 shows the scheme of a copropagating NLP, first conceived in [11], composed of a dispersion-shifted fiber (DSF), where the tunable pump, with power P_p, is coupled with the signal at the fiber input. The pump is then rejected by the optical bandpass filter (OBPF), which selects the signal spectrum, at the fiber output. The fiber, with length $L = 20$ km, is characterized by a Kerr coefficient $\gamma = 1.99\ \mathrm{W^{-1}\,km^{-1}}$, attenuation $\alpha = 0.2$ dB/km, and group velocity dispersion parameter $D = 4$ ps/nm/km.

The input signal consisted of a stream of individually polarized and intensity-modulated pulses, with peak power P_s and limited duration T_s. The SOP of each pulse was randomly chosen on the Poincaré sphere, so that the input signal was completely depolarized.

Signal and pump were placed at the fiber zero dispersion wavelength (zdw) λ_{zdw} and at wavelength λ_p, respectively, so that they propagate at different velocities. Thus, their walk-off at the fiber output is $T_d = D\Delta\lambda L$, where $\Delta\lambda = |\lambda_p - \lambda_{\mathrm{zdw}}|$. Since we fixed the fiber type and length (as well as the signal wavelength λ_{zdw}), we varied the walk-off T_d by tuning the pump wavelength λ_p. We varied $\Delta\lambda$ from 0 to 20 nm, still keeping signal and pump within the conventional telecom bandwidth (C-band). The limit case $\Delta\lambda = 0$ (i.e., $T_d = 0$) is

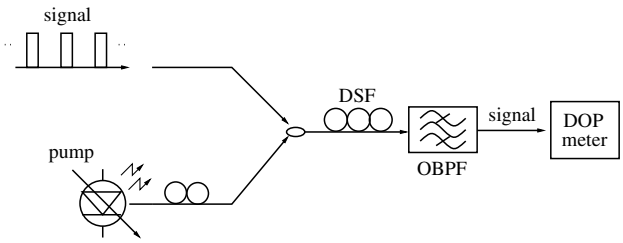

Fig. 1. System setup of a copropagating NLP.

mainly of theoretical interest, since signal and pump spectra would overlap each other. Anyway, $T_d = 0$ may be obtained with matched signal and pump group velocities (i.e., placed on opposite sides of the fiber zdw [12]).

In order to avoid pulse-to-pulse nonlinear interactions mediated by the pump, the signal pulses must be spaced by an interval at least equal to the walk-off delay T_d [10], as we did. Hence, the pulse repetition rate $R \le (T_d + T_s)^{-1}$ can become relatively small in the case of a large T_d (as well as for a large T_s). However, this is not a limiting factor for our study, where the main concern is the coherence time of the signal SOP to be repolarized (which coincides with T_s), rather than the transmission rate. In the following, we shall discuss how results presented in this work apply to any transmission rate of the signal.

The random birefringence of the fiber was taken into account by its polarization mode dispersion (PMD) coefficient $D_{\mathrm{PMD}} = 0.05\ \mathrm{ps/km^{1/2}}$ (typical of recent fibers). For the fiber length used here, D_{PMD} is small enough to make linear PMD effects negligible [10,13], while the random birefringence is such that propagation occurs within the so-called Manakov limit [1,10,13]. Hence, the evolution of the (unattenuated) signal and pump Jones vectors, $\mathbf{S}_s(z,t)$ and $\mathbf{S}_p(z,t)$, is governed by the following "Manakov equations" [13,14]:

$$\begin{cases} \frac{\partial \mathbf{S}_s}{\partial z} + \frac{1}{v_s}\frac{\partial \mathbf{S}_s}{\partial t} - j\frac{\beta_{2s}}{2}\frac{\partial^2 \mathbf{S}_s}{\partial t^2} \\ \quad = -j\frac{8}{9}\gamma e^{-\alpha z}[|\mathbf{S}_s|^2 + |\mathbf{S}_p|^2 + \mathbf{S}_p\mathbf{S}_p^{\dagger}]\mathbf{S}_s \\ \frac{\partial \mathbf{S}_p}{\partial z} + \frac{1}{v_p}\frac{\partial \mathbf{S}_p}{\partial t} - j\frac{\beta_{2p}}{2}\frac{\partial^2 \mathbf{S}_p}{\partial t^2} \\ \quad = -j\frac{8}{9}\gamma e^{-\alpha z}[|\mathbf{S}_p|^2 + |\mathbf{S}_s|^2 + \mathbf{S}_s\mathbf{S}_s^{\dagger}]\mathbf{S}_p \end{cases}. \tag{1}$$

where † stands for transpose-conjugate, $v_{s,p}$ represent the group velocities at the signal and pump wavelengths, respectively, and $\beta_{2s,p}$ are responsible for chromatic dispersion (although $\beta_{2s} = 0$ at λ_{zdw}). Moreover, in Eq. (1), $\mathbf{S}_{s,p}(z,t)$ are expressed in a polarization frame that follows the random evolution of the birefringence [13]. Note that in Eq. (1), it is only the last among the three nonlinear terms (i.e., the one with the †) that yields nonlinear polarization rotations, while the other two are responsible for self- and cross-phase modulations not affecting the SOP.

In order to better understand and describe geometrically the evolution of signal and pump SOPs, we should "translate" Eq. (1) into Stokes space (as done, e.g., in Refs. [13,14]), where signal and pump Stokes vectors propagate according to the following equations (of which Eq. (2) in [1] is a normalized version):

$$\begin{cases} \frac{\partial \mathbf{s}_s}{\partial z} + \frac{1}{2v_{\mathrm{wo}}}\frac{\partial \mathbf{s}_s}{\partial \tau} = \frac{8}{9}\gamma e^{-\alpha z}[\mathbf{s}_p \times \mathbf{s}_s] \\ \frac{\partial \mathbf{s}_p}{\partial z} - \frac{1}{2v_{\mathrm{wo}}}\frac{\partial \mathbf{s}_p}{\partial \tau} = \frac{8}{9}\gamma e^{-\alpha z}[\mathbf{s}_s \times \mathbf{s}_p] \end{cases}, \tag{2}$$

where $\times$ is the vector cross product and $\mathbf{s}_{s,p}(z,\tau) = s_{0s,p}(z,\tau)\hat{\mathbf{s}}_{s,p}(z,\tau)$ are the signal and pump Stokes vectors, with instantaneous SOP $\hat{\mathbf{s}}_{s,p}$ and intensities s_{0s} (variable, with maximum value P_s, for the signal) and $s_{0p} = P_p$ (constant, for the CW pump). Equation (2) is expressed in a time frame ($\tau \triangleq t - z/v_{\mathrm{ref}}$) moving at the reference velocity v_{ref} such that $v_{\mathrm{ref}}^{-1} \triangleq (v_s^{-1} + v_p^{-1})/2$. Within this framework, signal and pump can be seen as counterpropagating waves [11], despite the fact that the walk-off velocity v_{wo}, defined as $v_{\mathrm{wo}}^{-1} \triangleq v_s^{-1} - v_p^{-1}$, is tunable (in a limited range), rather than being fixed and relativistic. Similar to Eq. (1), $\mathbf{s}_{s,p}(z,\tau)$ are expressed in a polarization frame that follows the SOP variations due to the birefringence. Thus, the Stokes vectors are rotated so as to equalize the birefringence introduced by the fiber at the pump wavelength, from the input up to coordinate z [13]. Equation (2) is spherically isotropic, implying that LPA occurs in the same way toward any pump SOP [10]. To obtain the results that follow, we chose a linear horizontal input pump SOP, i.e., $\hat{\mathbf{s}}_p(0,\tau) = \hat{\mathbf{s}}_1$, without loss of generality. Despite the fact that Eq. (2) is a geometrically meaningful model for understanding the nonlinear polarization interactions, the simulation results were obtained by numerically solving the full Manakov-PMD propagation Eq. (1) in the Jones domain, including birefringence [not present in Eq. (1)]. Finally, Eq. (1) does not account for the four-wave mixing (FWM). We verified numerically that FWM effects (such as pump depletion) are safely negligible at the power levels employed in this work [10].

3. ROLE OF WALK-OFF IN LPA

Equation (2) is helpful in understanding the mechanism behind LPA, which we tackle here in a simplified picture. The plots in Fig. 2 show the evolution of the SOP of a single pulse along the NLP fiber during the nonlinear interaction with the pump. Since in Fig. 2 the Stokes vectors are expressed in the same framework as that of Eq. (2), the time-averaged pump SOP (blue dots) appears to be aligned with its input SOP $\hat{\mathbf{s}}_p(0) = \hat{\mathbf{s}}_1$ (blue vector in figure) at any position along the fiber. Each of the (red) dots, instead, is the time-averaged SOP of the signal pulse at a given position $0 \le z \le L$, i.e., it represents the direction of $\langle \mathbf{s}_s(z,\tau) \rangle$. As an example, Fig. 2 was obtained by injecting into the fiber a right-circular polarized pulse (i.e., $\hat{\mathbf{s}}_s(0) = \hat{\mathbf{s}}_3$; red vector in the figure). Here, we employ an equal signal and pump peak power, $P_s = P_p = 200$ mW.

We start from the simple case where signal and pump propagate at the same velocity $v_s = v_p$, and hence $v_{\mathrm{wo}}^{-1} = 0$; there is no walk-off and $T_d = 0$. The behavior of the signal SOP, reported in Fig. 2(a), can be simply explained in this case, since Eq. (2) allows a closed-form solution [12] from which it is well known that both the pulse SOP and that of the pump samples interacting with it evolve along the fiber according to a "carousel model" [14]. Thus, for $T_d = 0$, signal and pump rotate around a fixed pivot vector equal to their vector sum, $\mathbf{m} \triangleq \mathbf{s}_s + \mathbf{s}_p$, which is hence located midway between $\hat{\mathbf{s}}_3$ and $\hat{\mathbf{s}}_1$ in the present case of equal pump and pulse peak power. The circle thus described by the average pulse SOP (red dots), as seen in Fig. 2(a), can even make the signal SOP become aligned with the pump SOP ($\hat{\mathbf{s}}_1$) for certain values of the coordinate z and/or power [12], but still in a *polarization rotation regime*. Hence, the trajectory of the pulse SOP is subject to change with length, power, and input polarization.

This simple picture is broken whenever walk-off comes into play [15], as in Figs. 2(b) and 2(c). In order to understand the signal SOP motion, in this case, imagine adopting the "carousel model" described above, as an approximate local solution of Eq. (2). The walk-off between signal and pump is applied in discrete steps along the fiber in a split-step fashion, i.e., as if Eq. (2) were solved by alternating nonlinear polarization rotation (carousel) and walk-off. Starting at the

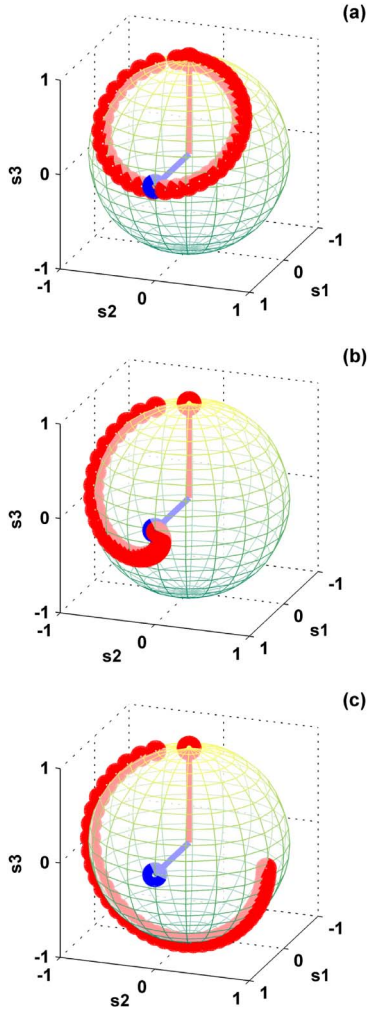

Fig. 2. Evolution of the average signal SOP along the NLP. Here, the input signal and pump SOP are rightcircular ($\hat{s}_3$) and linear-horizontal ($\hat{s}_1$), respectively (marked by red and blue vectors, in figure). A (a) too small ($\tau_d = 0$) or (c) too large ($\tau_d = 32$) walk-off induces polarization rotation, while true polarization attraction only occurs for (b) intermediate values ($\tau_d = 5$). (See Section 4 for the definition of τ_d.)

fiber input ($z = 0$), first, the signal and pump rotate around the pivot vector $\mathbf{m}(0) \triangleq \mathbf{s}_s(0) + \mathbf{s}_p(0)$ (constant, since we assume, in this step, that signal and pump travel at the same velocity). Then, at the end of each step, assume that the pump walks past the signal, due to walk-off. Thus, in the following step, the signal nonlinearly interacts with a "fresh" portion of the pump, whose SOP is the one it has at the fiber input, i.e., $\hat{\mathbf{s}}_1$, in our case. Hence, within this second nonlinear step, signal and pump rotate, according to the carousel model, around a new pivot $\mathbf{m}(\Delta z) \triangleq \mathbf{s}_s(\Delta z) + \mathbf{s}_p(0)$ (where Δz is the fiber step length). Since $\mathbf{s}_s(\Delta z)$ is closer to the input pump SOP compared to $\mathbf{s}_s(0)$, the arc covered by the signal SOP has a sharper curvature. The signal SOP thus follows arcs of a circle with increasing curvature and closer to the input pump SOP, which describe, in the limit ($\Delta z \to 0$), the spiral trajectory shown in Fig. 2(b). Such a motion, which we regularly observed in simulations, is a stable one, i.e., the signal SOP tends to collapse onto the input pump SOP. We refer to these conditions as the *polarization attraction regime*.

The picture just described holds as long as the walk-off is of the order of magnitude of the signal pulse duration. The case of a very large walk-off, shown in Fig. 2(c), can be explained by the rotation of the pulse SOP around the input pump SOP, as dictated by the first equation in Eq. (2), which governs the signal SOP evolution. Anyway, this case differs from the zero walk-off case, since, for a limited pulse duration and an extremely large walk-off, it is as if the signal pulse were infinitely short, and hence unable to perturb the pump SOP [through the second equation in Eq. (2), which governs the pump evolution], so that $\mathbf{s}_p$ is practically constant. Thus, with an extremely large walk-off, the pulse SOP undergoes a *polarization rotation regime*, where the rotation is performed around the pump SOP, hence following a larger trajectory, as compared to the zero walk-off case, where rotation occurs around an intermediate pivot.

As is clearly visible in Fig. 2, the average pulse SOP, starting at $\hat{\mathbf{s}}_3$, moves stably toward the pump SOP $\hat{\mathbf{s}}_1$, and hence evolves according to a *polarization attraction regime*, only for the intermediate case. On the contrary, the pulse SOP keeps rotating in a circle, i.e., undergoes a *polarization rotation regime*, in the other two cases. The two *polarization rotation regimes* never result in stable polarization attraction, since the pulse SOP evolves in circles (although an illusory attraction can occur, in the first case, for specific NLP parameters [12]).

The three dynamic pictures described above were regularly observed for any input pulse SOP other than $\hat{\mathbf{s}}_s(0) = \hat{\mathbf{s}}_3$. In particular, in the polarization attraction regime, the pulse SOP always stably evolves along a spiral trajectory around the pump SOP, whereas SOP rotation occurs in the polarization rotation regimes.

We can thus conclude that LPA is the joint effect of the Kerr nonlinearity and the walk-off, both occurring between pump and signal, in carefully balanced amounts [6], while a too large or too small walk-off simply yields polarization rotation.

4. SCALING LAWS AND THE NORMALIZED WALK-OFF

The effectiveness of polarization attraction, for the given NLP setup and parameters, depends primarily on the input pulse SOP, which can range from being parallel to the pump SOP (i.e., "already attracted") to being orthogonal to it (i.e., as already stated, "impossible to attract"). The overall NLP performance is thus quantified by the degree of polarization (DOP) of the output signal [10], evaluated as $\mathrm{DOP} = \|E[\langle \mathbf{s}_s(L,\tau)\rangle]\| / \langle s_{0s}(L,\tau)\rangle$, where $\langle\cdot\rangle$ and $E[\cdot]$ represent time- and statistical-average operators, respectively, while $\|\cdot\|$ is the Euclidean norm. To evaluate the DOP numerically, we averaged over 100 input pulse SOPs.

Figure 3(a) shows the output DOP of the signal after the nonlinear interaction with the pump as a function of the walk-off T_d, accumulated along the fiber. Different results are obtained for signals with different pulse durations, and Fig. 3 reports the plots obtained for the following values of T_s(ps): 1000, 400, 100, and 10. We see from Fig. 3(a) that an optimal walk-off T_d^* (and hence an optimal pump wavelength λ_p^*) exists that maximizes the effectiveness of LPA for each tested pulse duration. While such an optimal T_d^* (and the whole plot) depends on the signal pulse duration T_s, the best DOP value, $\mathrm{DOP}^* \cong 0.78$, is independent of it.

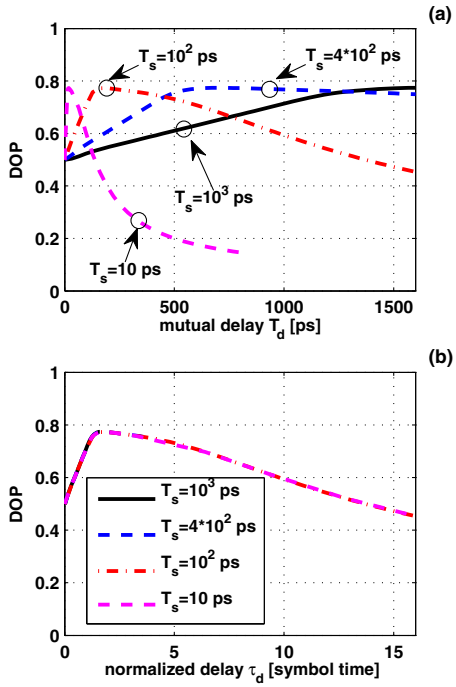

Fig. 3. Performance of a copropagating NLP: output signal DOP versus the mutual signal–pump walk-off delay T_d. (a) Results obtained for different pulse durations T_s obey a scaling law, so that (b) DOP only depends on the normalized delay $\tau_d \triangleq T_d/T_s$.

Moreover, T_d^* increases with the pulse duration T_s, meaning that the effectiveness of LPA fades away, i.e., DOP drops below DOP*, whenever T_d is too large or too small compared with the duration of the pulse to be attracted (which is consistent with the results discussed in the previous section).

The above results suggest that a scaling rule exists. This is indeed verified in Fig. 3(b), where the obtained DOP values are plotted versus a walk-off $\tau_d \triangleq T_d/T_s$, normalized to the pulse duration. Thus, each curve in Fig. 3(a) can be obtained by rescaling a single curve, visible in Fig. 3(b), which summarizes the LPA performance for any pulse duration at the chosen power level. Hence, the curve in Fig. 3(b) demonstrates that a NLP can effectively operate even on signals with a short coherence time of their SOP (i.e., a SOP that rapidly changes from pulse to pulse) and does not require a long response time [7], provided that a copropagating pump is employed [10] with an appropriate walk-off. At the same time, Fig. 3 yields the rule for controlling LPA transients by properly selecting the pump wavelength. The optimal walk-off is $\tau_d^* \cong 1.75$ and depends on signal power, as discussed further.

The scaling rule, just obtained numerically, can be verified analytically. By introducing in Eq. (2) the change of time scale $\tau' = \tau/T$, so that $\mathbf{s}'_{s,p}(z,\tau') = \mathbf{s}_{s,p}(z,\tau/T)$ are compressed versions (if $0 < T < 1$) of the signal pulse and of the pump, $\mathbf{s}'_s(z,\tau')$ and $\mathbf{s}'_p(z,\tau')$ obey a set of equations identical to Eq. (2), provided that the walk-off velocity v_{wo} is replaced by $v'_{\mathrm{wo}} = T \cdot v_{\mathrm{wo}}$. This implies that the output signal evolution and, hence, its SOP and the corresponding overall DOP are the same as those obtained by solving Eq. (2) for a rescaled walk-off velocity v'_{wo}, and hence for a rescaled delay $\tau'_d = L/v'_{\mathrm{wo}} = T_d/T$. As a consequence, by choosing the time-scaling factor equal to the pulse duration, i.e., $T = T_s$, all the curves in Fig. 3(a) coincide, as demonstrated in Fig. 3(b).

The practical implication of this result is that given the NLP parameters and the pulse duration, the optimal $T_d^* \cong 1.75 \cdot T_s$ can be reached by placing the pump at an optimal wavelength distance $\Delta\lambda^* = T_d^*/(D \cdot L)$ from the signal. On the other hand, for a given pump wavelength, and hence a fixed $\Delta\lambda$ (and T_d), the effectiveness of the NLP device is optimal only for a pulse duration $T_s^* \cong T_d/1.75$. In any case, LPA effectively occurs only for a limited range of walk-off values; e.g., in the present case of system parameters, the results in Fig. 3(b) show that $1 < \tau_d < 6$ is required to achieve DOP > 0.7. Such a range represents a sort of *polarization attraction interval* within which LPA could be considered effective.

5. ROLE OF POWER IN LPA

Until now, we concentrated our attention only on the role of walk-off in LPA. In order to study how the polarization attraction regime changes as a function of the strength of Kerr interactions, we varied the signals' peak power, P_s and P_p, keeping them equal, $P_s = P_p$. The results in Fig. 4 show that by increasing power, and hence the amount of nonlinearity, the best DOP, i.e., the NLP performance, increases, while the optimal walk-off is always about twice the pulse duration T_s. For a walk-off much smaller than the optimal τ_d^* (left side of the plots), all curves overlap. For a walk-off much larger than τ_d^* (right side of the plots), the performance of the NLP increases by increasing the signal power, and apparently tends to flatten, as a function of τ_d. However, for very large normalized walk-off values ($\tau_d \simeq 550$), the DOP significantly decreases, even for large powers, as seen in Fig. 4. These results further prove that an optimal walk-off exists, even at the largest affordable power levels. While it is true that the polarization attraction regime turns into the polarization rotation regime with a smooth transition and without physical discontinuities, an effective *polarization attraction interval* can always be identified, which increases by increasing the signal power, as shown in Fig. 4. As an example, a DOP $\geq$ 0.7 can be obtained either by fine tuning the normalized walk-off ($1 < \tau_d < 6$) for signal power $P_s = P_p = 0.2$ W, or from a wide range of values ($1 < \tau_d < 600$) for signal power $P_s = P_p = 2$ W.

Despite the fact that the values of normalized walk-off tested here, between 0 and 600, are still small when compared with the walk-off given by the counterpropagating geometry,

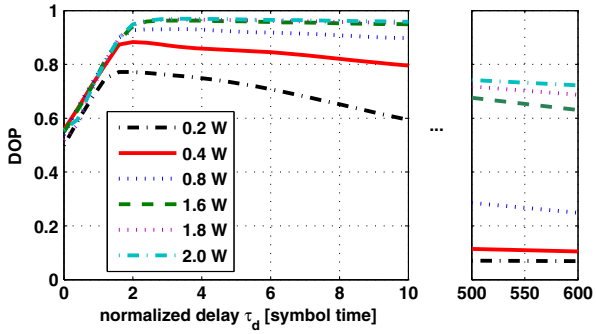

Fig. 4. Performance of a copropagating NLP: DOP versus τ_d for different values of the signal power ($P_s = P_p$). The six tested values are 0.2, 0.4, 0.8, 1.6, 1.8, and 2 W.

the above argument explains why a counterpropagating NLP is effective only for long and powerful signals. High signal power is needed to enlarge the *polarization attraction interval*, while long signal durations are needed to decrease the normalized walk-off, so that it is closer to the *polarization attraction interval*. In fact, while a copropagating pump allows us to control the normalized walk-off τ_d by tuning the pump wavelength ($\Delta\lambda$), with a counterpropagating pump, τ_d can change only due to the pulse duration T_s. For a counterpropagating NLP where the fiber length is around 10 km and power levels are around 1 W (i.e., conditions similar to those adopted, e.g., in [9]), the polarization attraction regime occurs only for signals whose duration is at least in the order of 1 μs. It should be noted, however, that, still referring to the setup described above, the (relativistic) walk-off is some tens of microseconds, which makes the counterpropagating NLP operate far from optimal conditions, since for a 1 μs pulse, τ_d is much larger than the optimal walk-off, which is always in the range of a few pulse durations, even at large power levels. Anyway, as shown in [9], the signal Stokes vector evolves along a spiral trajectory, in all respects similar to the one observed in Fig. 2(b). However, for signals whose duration is much shorter than a microsecond, the counterpropagating NLP works in the polarization rotation regime, where the signal Stokes vector rotates around the pump Stokes vector, which we verified, as depicted in Fig. 2(c).

6. CONCLUSIONS

To conclude, we characterized the performance of a copropagating NLP by measuring the output signal DOP as a function of the walk-off T_d between the attracting CW pump and an attracted signal pulse. We demonstrated that a scaling rule exists, so that the optimal performance (DOP) can be achieved for any pulse duration, provided that the walk-off is tuned accordingly by placing the pump at an optimal wavelength. As a consequence, we showed that the *polarization attraction regime* occurs only when Kerr nonlinearity and walk-off are carefully balanced. Although we considered pulse duration typical of telecom links, the results obtained in this work apply to modulated signals with any transmission rate R_b, provided that a proper duty cycle is chosen. In fact, for a pulse repetition rate $R = R_b$, the symbol period obeys $T_b \geq T_d + T_s$, while the duty cycle of transmitted bits is $d = R_b T_s \leq (\tau_d + 1)^{-1}$, whose upper bound depends only on the normalized walk-off τ_d. Hence, for any R_b, a pulse duration $T_s = d^*/R_b \leq (R_b(\tau_d^* + 1))^{-1}$ can be chosen in agreement with the optimal normalized walk-off τ_d^* that optimizes the NLP performance. Since, from Fig. 4, it is typically $\tau_d^* \lesssim 2$, a standard $d = 0.33$ guarantees that good repolarization of each single bit can be achieved, avoiding pulse-to-pulse nonlinear interactions. As an example, in [4] a copropagating NLP was applied to repolarize a 10 Gbit/s return-to-zero (33% return-to-zero) on–off keying signal, whose SOP was randomly changed from bit to bit. Moreover, we demonstrated that a copropagating NLP is more flexible and power efficient compared with a traditional counterpropagating NLP. The counterpropagating configuration can indeed be seen as the (suboptimal) limit case of the copropagating configuration for an extremely large and relativistic walk-off.

REFERENCES

1. G. Millot and S. Wabnitz, "Nonlinear polarization effects in optical fibers: polarization attraction and modulation instability [Invited]," J. Opt. Soc. Am. B **31**, 2754–2768 (2014).
2. Y. Su, L. Mller, C. Xie, R. Ryf, X. Liu, X. Wei, and S. Cabot, "Ultra high-speed data signals with alternating and pairwise alternating optical phases," J. Lightwave Technol. **23**, 26–31 (2005).
3. P. Morin, J. Fatome, C. Finot, S. Pitois, R. Claveau, and G. Millot, "All-optical nonlinear processing of both polarization state and intensity profile for 40 Gbit/s regeneration applications," Opt. Express **19**, 17158–17166 (2011).
4. M. Barozzi and A. Vannucci, "Lossless polarization attraction of telecom signals: application to all-optical OSNR enhancement," J. Opt. Soc. Am. B **31**, 2712–2720 (2014).
5. V. C. Ribeiro, R. S. Luís, J. M. D. Mendinueta, B. J. Puttman, A. Shahpari, N. J. C. Muga, M. Lima, S. Shinada, N. Wada, and A. Teixeira, "All-optical packet alignment using polarization attraction effect," IEEE Photon. Technol. Lett. **27**, 541–544 (2015).
6. M. Barozzi and A. Vannucci, "Optimal pump wavelength placement in lossless polarization attraction," in *Proceedings of Fotonica* (AEIT, 2013).
7. V. V. Kozlov, J. Fatome, P. Morin, S. Pitois, G. Millot, and S. Wabnitz, "Nonlinear repolarization dynamics in optical fibers: transient polarization attraction," J. Opt. Soc. Am. B **28**, 1782–1791 (2011).
8. M. Barozzi and A. Vannucci, "Performance characterization and guidelines for the design of a counter-propagating nonlinear lossless polarizer," J. Opt. Soc. Am. B **30**, 3102–3112 (2013).
9. M. Barozzi, A. Vannucci, and D. Sperti, "Lossless polarization attraction simulation with a novel and simple counterpropagation algorithm for optical signals," J. Eur. Opt. Soc. **7**, 12042 (2012).
10. V. V. Kozlov, M. Barozzi, A. Vannucci, and S. Wabnitz, "Lossless polarization attraction of copropagating beams in telecom fibers," J. Opt. Soc. Am. B **30**, 530–540 (2013).
11. S. Pitois and M. Haelterman, "Optical fiber polarization funnel," in *Nonlinear Guided Waves and Their Applications*, OSA Technical Digest Series (Optical Society of America, 2001), pp. 278–280.
12. V. V. Kozlov, K. Turitsyn, and S. Wabnitz, "Nonlinear repolarization in optical fibers: polarization attraction with copropagating beams," Opt. Lett. **36**, 4050–4052 (2011).
13. P. K. A. Wai and C. R. Menyuk, "Polarization mode dispersion, decorrelation, and diffusion in optical fibers with randomly varying birefringence," J. Lightwave Technol. **14**, 148–157 (1996).
14. A. Bononi, A. Vannucci, A. Orlandini, E. Corbel, S. Lanne, and S. Bigo, "Degree of polarization degradation due to cross-polarization modulation and its impact on polarization-mode dispersion compensator," J. Lightwave Technol. **21**, 1903–1913 (2003).
15. A. Vannucci, A. Bononi, A. Orlandini, E. Corbel, J. Thiéry, S. Lanne, and S. Bigo, "A simple formula for the degree of polarization degraded by XPM and its experimental validation," in *Proceedings of Optical Fiber Communication (OFC 2003)* (IEEE, 2003), Vol. **2**, pp. 498–499.